Mechanistic investigation of the ameliorative effect of liquiritin on hypoxia/reoxygenation-induced cardiomyocyte injury based on network pharmacology and *in vitro* validation

HAOYING LI[1*], LINLIN BU[1*], XIAOQI SUN[1], XI CHU[2], YUCONG XUE[1], MUQING ZHANG[3], JING SHI[2], YANSHUANG LIU[4,5], SHENGJIANG GUAN[3], XUE HAN[1] and HONGFANG WANG[1]

[1]School of Pharmacy, Hebei University of Chinese Medicine, Shijiazhuang, Hebei 050200;
[2]Department of Pharmacy, The Fourth Hospital of Hebei Medical University, Shijiazhuang, Hebei 050011;
[3]Affiliated Hospital, Hebei University of Chinese Medicine, Shijiazhuang, Hebei 050000;
[4]College of Integrative Medicine, Hebei University of Chinese Medicine, Shijiazhuang, Hebei 050200;
[5]College of Integrative Medicine, Hebei Medical University, Shijiazhuang, Hebei 050000, P.R. China

Received September 10, 2023; Accepted December 18, 2023

DOI: 10.3892/etm.2024.12405

Abstract. Liquiritin (LIQ) is a flavonoid known for its cardioprotective properties, extracted from *Glycyrrhiza uralensis* Fisch. The purpose of the present study was to investigate the protective mechanism of LIQ against hypoxia/reoxygenation (H/R) injury through *in vitro* experiments, with the goal of enhancing its pharmacological effects. Initially, network pharmacology was employed to explore the targets and mechanisms of LIQ. Subsequently, an *in vitro* H/R model was established using H9c2 cells. Potential targets for LIQ and myocardial ischemia-reperfusion injury (MIRI) were identified through online databases. The STRING, Cytoscape and DAVID databases were used to extract intersecting targets and mechanisms. *In vitro* experiments were conducted to validate these findings, assessing cardiac enzymes, oxidative stress indicators, mitochondrial fluorescence, apoptotic fluorescence, inflammation and related protein expression. The network pharmacological analysis revealed that the protective effects of LIQ on MIRI involve oxidative stress, inflammation and apoptosis. The results of *in vitro* experimental validation demonstrated that LIQ significantly reduced the activities of lactated dehydrogenase and creatine kinase isoenzyme-MB ($P<0.05$ or 0.01), as well as the level of malondialdehyde ($P<0.01$). It also inhibited the production of reactive oxygen species ($P<0.01$), the release of inflammatory factors ($P<0.05$ or 0.01) and apoptosis ($P<0.01$). By contrast, the LIQ pre-treatment group exhibited a significant increase in mitochondrial membrane potential level ($P<0.05$ or 0.01) and the activities of antioxidant enzymes superoxide dismutase, catalase and glutathione peroxidase ($P<0.05$ or 0.01). Furthermore, LIQ reduced the protein expressions of TNF-α receptor type 1 (TNFR1) and MMP9, along with the level of NF-κB phosphorylation ($P<0.05$ or 0.01). In conclusion, LIQ mitigated H/R-induced cardiomyocyte injury through mechanisms that may involve antioxidants, anti-apoptotic effects, protection against mitochondrial damage and suppression of inflammatory levels. These effects are achieved via inhibition of the TNFR1/NF-κB/MMP9 pathway.

Correspondence to: Professor Shengjiang Guan, Affiliated Hospital, Hebei University of Chinese Medicine, 389 Zhongshan East Road, Chang'an, Shijiazhuang, Hebei 050000, P.R. China
E-mail: guanshengjiang123@126.com

Ms. Hongfang Wang, School of Pharmacy, Hebei University of Chinese Medicine, 3 Xingyuan Road, Luquan, Shijiazhuang, Hebei 050200, P.R. China
E-mail: wanghongfang@hebcm.edu.cn

[*]Contributed equally

Key words: liquiritin, network pharmacology, cellular experiments, H9c2 cells, hypoxia/reoxygenation, $CoCl_2$

Introduction

Acute myocardial infarction (AMI) is a prevalent cardiovascular disease with a high morbidity and mortality rate. It is characterized by the blockage of coronary arteries, leading to restricted blood supply to the heart and resulting in tissue hypoxia. Following an AMI, various strategies are employed to reduce the area of myocardial infarction and improve clinical outcomes. These strategies include early primary percutaneous coronary intervention or timely and successful myocardial reperfusion using thrombolytic therapy. However, the process of restoring myocardial blood flow and reoxygenation can have detrimental effects on the therapeutic outcome, leading to myocardial ischemia-reperfusion injury (MIRI) (1). As a result, hypoxia/reoxygenation (H/R) plays a crucial role in the pathological process associated with MIRI (2). The most commonly used method to simulate MIRI *in vitro* involves establishing a cellular H/R model (3).

As research into the underlying pathophysiology of MIRI progresses, the pathological mechanisms are gradually becoming clearer. These mechanisms primarily involve

the excessive production of reactive oxygen species (ROS), autophagy, apoptosis, necroptosis and the generation of inflammatory factors. Collectively, these processes contribute to myocardial cell death and subsequent myocardial dysfunction (4-7). During MIRI, cardiomyocytes are stimulated to produce large amounts of ROS, resulting in oxidative damage and significant mitochondrial dysfunction. Concurrently, the mitochondrial apoptotic pathway is activated, leading to irreversible apoptosis (8). Despite ongoing efforts, MIRI remains a significant clinical challenge with no definitive therapeutic solution. Therefore, there is an urgent need to further understand the pathogenesis and explore novel treatment strategies to improve clinical outcomes for patients with AMI.

Glycyrrhiza uralensis Fisch, a traditional Chinese medicinal plant, holds significant commercial and medicinal value as both a medicine and a food source (9-11). Within this plant, a flavonoid known as liquiritin (LIQ) has been identified and its chemical structure has been determined (Fig. 1). LIQ demonstrates various pharmacological activities, including cardioprotective effects (12). A previous study reported the potential of LIQ as a therapeutic strategy for repairing injured myocardium by reducing the expression of inflammatory mediators, inhibiting cardiac oxidative stress and preventing apoptosis (13). Furthermore, a study indicated that LIQ protects the myocardium from H/R injury by mitigating mitochondrial Ca^{2+} overload and preserving mitochondrial mass (14). A research group has previously validated the protective effect of LIQ in a rat model of myocardial infarction (15). The current study aimed to investigate the specific mechanisms through which LIQ safeguards cardiomyocytes from H/R injury using *in vitro* assays, contributing to the advancement of targeted drugs for treating cardiovascular diseases.

Network pharmacology is an interdisciplinary approach that combines bioinformatics and pharmacology to systematically uncover the connections between Chinese medicines, compounds and various diseases. Computational integration and analysis of data enable the exploration of drug action mechanisms (16). Based on the aforementioned theoretical background, the present study innovatively integrated network pharmacology and cellular experiments to elucidate the mechanism of action of LIQ in preventing and treating cardiomyocyte H/R injury. Specifically, network pharmacological methods were employed to preliminarily predict the key targets and biological pathways involved in LIQ therapy for MIRI. Subsequently, cellular experiments are conducted to demonstrate specific underlying mechanisms through various perspectives including oxidative stress, apoptosis, inflammation, mitochondrial damage and molecular pathways. The present study provided a scientific foundation for understanding the molecular-level protective effect of LIQ on myocardium.

Materials and methods

Database and analysis software. Traditional Chinese Medicine Systems Pharmacology Database v2.3 (TCMSP; https://old.tcmsp-e.com/index.php); UniProt database v2020_01 (https://www.uniprot.org/); Swiss Target Prediction v2019 (http://www.swisstargetprediction.ch/); PharmMapper v2017 (http://www.lilab-ecust.cn/pharmmapper/index.html); GeneCards database v5.5 (https://www.genecards.org/); E Venn Diagram website (http://www.ehbio.com/test/venn/); STRING database v11.0 (https://string-db.org/); DAVID v6.8 (https://david.ncifcrf.gov/tools.jsp); Microbiology website (http://www.bioinformatics.com.cn/) and Cytoscape software (version 3.7.2) (17) were employed.

Network pharmacology methods

Acquisition of potential targets for LIQ and MIRI. The compound characteristics and physicochemical parameters of LIQ were obtained using CAS No. 551-15-5 from the TCMSP. Additionally, the corresponding targets were obtained. The SDF files of LIQ were acquired from the PubChem database and subsequently imported into the Swiss Target Prediction and PharmMapper websites to predict the targets associated with LIQ. The results from these three databases were then consolidated. The UniProt database was used to gather the gene names of the respective LIQ targets, with a species restriction set to 'Homo sapiens'. Finally, a search was conducted in the GeneCards database using 'Myocardial ischemia-reperfusion injury' as a keyword to identify potential targets.

Drug-disease common target screening and interoperability network construction. Venn diagrams were created by intersecting the targets associated with MIRI and those associated with LIQ, using an online Venn diagram tool. This facilitated the identification of common targets shared between the drug and the disease. Following this, a protein-protein interaction (PPI) network was constructed for these common targets using the STRING 11.0 database. The resulting TSV files were downloaded and then imported into the Cytoscape software for visualization.

Core target screening. The 'NetworkAnalyzer' plug-in within Cytoscape software was used to analyze the Degree values of each target in the PPI network. This analysis enabled the identification of core targets by prioritizing them based on their Degree values. It is important to highlight that targets with higher Degree values hold greater significance within the network.

Gene Ontology (GO) and Kyoto Encyclopedia of Genes and Genomes (KEGG) enrichment. The common targets were imported into the DAVID database to gain deeper insights into the functions of the common targets resulting from the intersection of LIQ and MIRI. Following this, GO and KEGG enrichment analyses were performed using the DAVID database by entering a list of target gene names and specifying the species as human. The GO analysis encompassed biological process (BP), cellular component (CC) and molecular function (MF) categories. The obtained results were subsequently analyzed and visualized using the Microbiology website.

Chemicals. LIQ was obtained from Chengdu Alfa Biotechnology Co., Ltd. $CoCl_2$ was purchased from Toronto Research Chemicals. Cell Counting Kit-8 (CCK-8; cat. no. G02111) was acquired from Dongren Chemical Technology Co., Ltd. High-glucose Dulbecco's modified Eagle medium (DMEM; cat. no. 12430047) and fetal bovine serum (FBS; cat. no. 10093188) were purchased from Gibco (Thermo

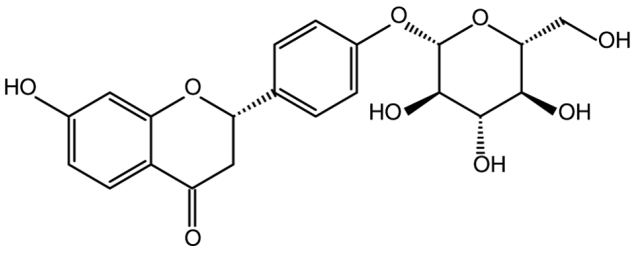

Figure 1. Chemical structure of liquiritin.

Fisher Scientific, Inc.). TNF-α (cat. no. 88-7340-88) and IL-6 (cat. no. 88-50625-88) ELISA kits were obtained from Thermo Fisher Scientific, Inc. The remaining ELISA kits, including lactated dehydrogenase (LDH; cat. no. A02022), creatine kinase isoenzyme-MB (CK-MB; cat. no. H197-1-1), superoxide dismutase (SOD; cat. no. A00132), catalase (CAT; cat. no. A007-11), glutathione peroxidase (GSH-Px; cat. no. A005-1-2) and malondialdehyde (MDA; cat. no. A00311), were from Nanjing Jiancheng Bioengineering Institute. Unless stated otherwise, all other reagents used in this experiment were purchased from Sigma-Aldrich (Merck KGaA).

Cell culture. H9c2 cells (Bluefbio Biotechnology Development, Inc.; cat. no. BFN60804388) were maintained in high-glucose DMEM supplemented with 10% FBS and 100 U/ml penicillin/streptomycin. The cells were incubated at 37˚C, 5% CO_2 and 95% air in an incubator. The culture medium was refreshed every 2-3 days. When the cells reached ~70-80% confluence, they were detached using 0.25 g/l trypsin, passaged and diluted to the appropriate cell suspension concentration. Subsequently, the cells were cultured in 96-, 24- and 6-well plates until they adhered.

Proliferation inhibition assay of H9c2 cells by LIQ. H9c2 cells cultured in 96-well plates were exposed to various concentrations of LIQ (1, 3, 10, 30, 100 and 300 μmol/l). After a 24-h incubation period, 10 μl of CCK-8 solution was added and absorbance was measured at 450 nm using an enzyme labeling instrument (Thermo Scientific Varioskan LUX; Thermo Fisher Scientific, Inc.). The protective concentrations of LIQ were determined based on CCK-8 calculations, confirming 3 and 10 μmol/l as the effective concentrations.

Determination of hypoxic dose and reoxygenation time. Experiments were conducted with H9c2 cells seeded in 96-well plates. The cells were exposed to different concentrations (200, 400, 600, 800 and 1,000 μmol/l) of $CoCl_2$ solutions prepared in complete medium for 24 h. The optimal hypoxic concentration was determined based on the results obtained from the CCK-8 assay. Following the hypoxic phase, the cells were incubated in complete medium for varying time intervals (1, 2, 3, 4, 5 and 6 h) to determine the appropriate reoxygenation duration. The optimal reoxygenation time was established using the results from the CCK-8 kit. In summary, the H/R injury model was established by subjecting the cells to 400 μmol/l $CoCl_2$-induced hypoxia for 24 h, followed by reoxygenation for 3 h. The experimental groups were categorized as follows: i) Control (CON); ii) H/R; iii) H/R + 3 μmol/l (L-) LIQ; iv) H/R + 10 μmol/l (H-)LIQ; v) LIQ (10 μmol/l).

Measurement of LDH and CK-MB. Following the aforementioned treatment, the cell culture medium supernatant was collected. Subsequently, the levels of LDH and CK-MB were measured in each group following the instructions provided with the respective kits.

Measurement of SOD, CAT, GSH-Px and MDA activities. At the conclusion of the experiment, the cells were scraped and resuspended in 500 μl of PBS solution. A cell homogenate was then prepared and the levels of SOD, CAT, GSH-Px and MDA were measured using the respective kits, following the provided instructions.

Measurement of ROS generation. 2,7-Dichlorodihydrofluorescein diacetate (DCFHDA, Cayman Chemical Company; cat. no. 85155) itself does not emit green fluorescence. However, intracellular ROS oxidizes the non-fluorescent DCFH to green-fluorescent DCF. The intensity of the resulting green fluorescence indirectly reflects the level of intracellular ROS. H9c2 cells were seeded in 24-well culture plates and allowed to grow until they reached ~80% confluence. Subsequently, the cells were treated as required. After the treatment, the cells were rinsed twice with PBS and incubated with 10 μmol/l DCFH-DA dye at 37˚C for 20 min. Images were captured using a fluorescence microscope (Nikon Eclipse C1; Nikon Corporation) and the green fluorescence intensity was semi-quantitatively analyzed using ImagePro Plus 6.0 software (Media Cybernetics, Inc.). The green fluorescence intensity was then analyzed semi-quantitatively and statistically for each sample within each group.

Measurement of mitochondrial membrane potential (MtMP). Rhodamine 123 (Shanghai Yuanye Biotechnology Co., Ltd; cat. no. S19123) is a fluorescent dye that selectively accumulates in mitochondria based on their transmembrane potential. When the cells reached ~80% confluence, various conditioned media were applied as per the experimental requirements. Following treatment, the cells were washed twice with PBS and then incubated at 37˚C for 20 min in a serum-free medium containing 100 μg/l Rh123. The green fluorescence observed around the nuclei indicated the uptake of Rh123 by the mitochondria. The green fluorescence intensity, representing Rh123 uptake by mitochondria, was semi-quantitatively analyzed using ImagePro Plus 6.0 software (Media Cybernetics, Inc.). Statistical analysis was conducted on the green fluorescence intensity for each sample within each group.

Measurement of intracellular inflammatory cytokines. H9c2 cells were seeded in 6-well plates and treated according to the experimental group requirements once they reached the desired confluency. The treated cells were collected as the test specimens. ELISA procedures were carried out following the instructions provided with the respective kits. After the reaction was completed, the absorbance values of each well were measured using a multifunctional microplate reader. The levels of TNF-α and IL-6 were determined following the provided kit instructions.

Measurement of apoptosis. H9c2 cells were cultured in 24-well plates and treated as required once they reached the desired density. Hoechst-33258 dye (Beijing Solarbio Science & Technology Co., Ltd; cat. no. IH0060) buffer at a concentration of 5 mg/l was applied to the cells, followed by a 15-min incubation in a cell incubator. The nuclei of apoptotic cells displayed either condensed solidified forms or granular fluorescence. Quantification of apoptotic cells was performed using ImagePro Plus 6.0 software (Media Cybernetics, Inc.).

Western blotting. The core targets and key signaling pathways predicted through network pharmacology were validated using the western blotting. H9c2 cells were seeded in 6-well plates and treated according to the experimental requirements. The cells were washed twice with pre-cooled PBS and then lysed using cell lysate (Beijing Solarbio Science & Technology Co., Ltd.; cat. no. R0020). The lysates were centrifuged at 12,000 x g for 10 min at 4˚C. The supernatant was quantified using the BCA method. Total protein (10 μg) was separated using 10% SDS-PAGE and transferred onto PVDF membranes. The PVDF membranes were subsequently incubated in 5% skimmed milk powder for 1.5 h to block nonspecific binding at 37˚C. Next, the membranes were incubated overnight at 4˚C with the corresponding primary antibodies, as follows: TNF-α receptor type 1 (TNFR1, Affinity Biosciences; diluted at 1:1,000; cat. no. AF0282), NF-κB (Affinity Biosciences; diluted at 1:1,000; cat. no. BF8005), phosphorylated (p-)NF-κB (Affinity Biosciences; diluted at 1:1,000; cat. no. AF2006), MMP9 (Affinity Biosciences; diluted at 1:1,000; cat. no. AF5228) and β-actin (Affinity Biosciences; diluted at 1:10,000; cat. no. AF7018). The following day, the membranes were washed three times with TBST (0.1% Tween 20) for an average of 10 min per wash, followed by incubation with the corresponding secondary antibody at room temperature for 1 h. After an additional three washes, grayscale values were measured using Visioncapt software (Fusion FX5 Spectra; Wilbur Bioimaging).

Statistical analysis. GraphPad Prism 8.0.2 software (Dotmatics) was used for statistical analyses. Data were presented as mean ± standard error of mean and one-way analysis of variance followed by Tukey's post hoc test was employed to assess statistically significant differences between groups. $P<0.05$ was considered to indicate a statistically significant difference.

Results

Network pharmacology analysis predicts results

Physicochemical properties of LIQ. The data pertaining to the physicochemical and pharmacological molecular properties of LIQ were sourced from the TCMSP database. Drug-like properties (DL) serve as a valuable indicator for assessing the potential of an ingredient in drug development, while oral availability (OB) is employed to gauge the ease of absorption of the ingredient into the bloodstream. The obtained OB value was 65.69% and the DL properties were measured at 0.74. These results demonstrated that LIQ exhibited an OB value of ≥30% and a DL value of ≥0.18, indicating its strong potential for drug development, as it is well-absorbed and possesses favorable drug-like properties.

LIQ and MIRI's potential target acquisition. A comprehensive analysis identified 315 targets for LIQ through predictions derived from the TCMSP database, Swiss Target Prediction and PharmMapper databases. In parallel, 1,052 targets for MIRI were predicted based on data from the Genecards database. The intersection of these two datasets revealed a total of 99 shared targets, as illustrated in Fig. 2A. Detailed information pertaining to specific target sites can be found in Fig. 2B.

Construction of PPI networks. The PPI network was established by entering the shared targets into the STRING database with subsequently analysis to identify its core network, as depicted in Fig. 2C. Within this core network, the top 10 targets were identified (Fig. 2D), which included AKT1, cystatin protease 3 (CASP3), albumin (ALB), proto-oncogene tyrosine-protein kinase Src (SRC), MMP9, heat shock protein 90α family class A member 1 (HSP90AA1), membrane-linked protein A5 (ANXA5), prostaglandin-endoperoxide synthase 2 (PTGS2), nitric oxide synthase 3 (NOS3) and peroxisome proliferator-activated receptor γ (PPARG). MMP9 was selected as the primary focus of this research among these targets.

GO functional analysis and KEGG pathway analysis. GO analysis, conducted using the DAVID database, yielded a total of 541 GO entries. Examination of the 394 BP categories unveiled the involvement of processes such as hypoxia, apoptosis, inflammation and oxidative stress. Within the CC entries, a total of 48 terms were enriched, primarily connected to extracellular exosomes, extracellular regions, plasma membranes, cytosols and mitochondria. The MF entries were also enriched, featuring 99 terms primarily associated with functions such as identical protein binding, peptidase activity, protein binding, zinc ion binding and cysteine-type endopeptidase activity involved in the execution phase of apoptosis, as depicted in Fig. 3A-C.

The KEGG pathway enrichment analysis identified a total of 125 pathways ($P<0.01$). These pathways were predominantly related to lipid and atherosclerosis, pathways in cancer, the TNF signaling pathway, the IL-17 signaling pathway and apoptosis. To enhance clarity, the top 20 pathways were selected for visualization, as depicted in Fig. 3D. Notably, among these pathways, 11 targets of LIQ were found to be involved in the regulation of the TNF signaling pathway, with the core target MMP9 among them. Details of the predicted targets associated with the TNF signaling pathway can be found in Fig. 4.

Effect of LIQ on cell viability. As shown in Fig. 5A, no significant changes in cell survival were observed when H9c2 cells were exposed to various concentrations of LIQ. To determine the optimal pre-protective concentrations for LIQ, 3 μmol/l and 10 μmol/l were selected. As depicted in Fig. 5B, cell viability decreased as the $CoCl_2$ concentration increased when H9c2 cells were subjected to varying $CoCl_2$ concentrations. To maintain cell survival at ~50% following hypoxia/reoxygenation, 400 μmol/l of $CoCl_2$ was selected to induce hypoxia ($P<0.01$), followed by a 3-h reoxygenation period (Fig. 5C;

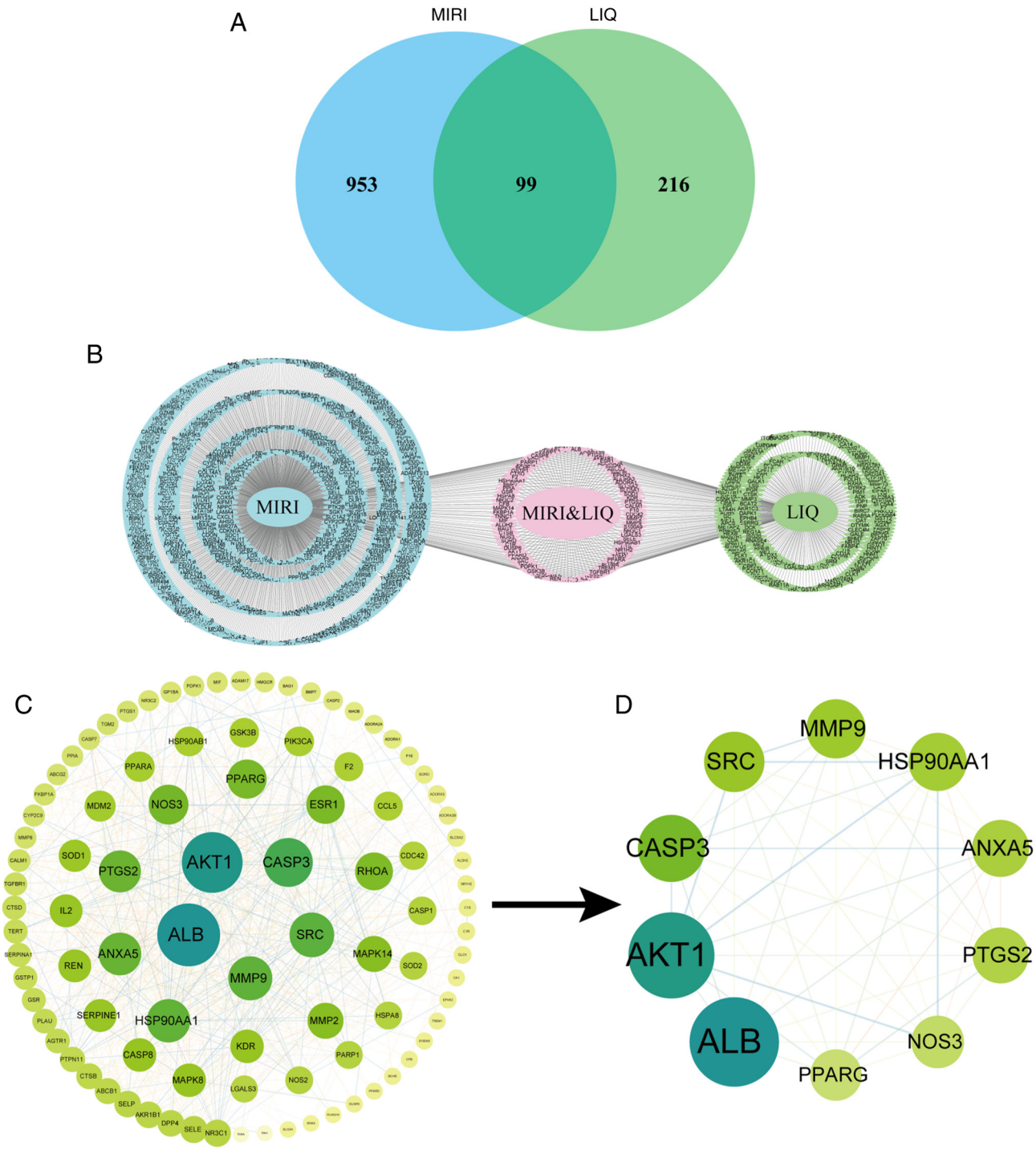

Figure 2. Core target analysis diagram on overlapping focal points of LIQ for MIRI. (B) Composite target display and (A) Venn diagram of LIQ and MIRI-related targets. (C) Core Target Interaction Network Diagram. (D) Top 10 targets of the core targets. LIQ, liquiritin; MIRI, myocardial ischemia-reperfusion injury; AKT1, Protein Kinase B α; CASP3, cystatin protease 3; ALB, albumin; SRC, proto-oncogene tyrosine-protein kinase Src; MMP9, Matrix metalloproteinase-9; HSP90AA1, heat shock protein 90α family class A member 1; ANXA5, membrane-linked protein A5; PTGS2, prostaglandin-endoperoxide synthase 2; NOS3, nitric oxide synthase 3; PPARG, peroxisome proliferator-activated receptor γ.

P<0.01). As illustrated in Fig. 5D, the viability of cells in the H/R group was significantly lower than that in the CON group (P<0.01). However, LIQ pre-treatment effectively mitigated the inhibitory effect of $CoCl_2$ on H9c2 cell viability (P<0.01).

Effect of LIQ on the release of LDH and CK-MB. As depicted in Fig. 6A and B, the levels of LDH and CK-MB exhibited a significant increase in the H/R group compared with the CON group (P<0.01). However, treatment with LIQ resulted in a notable reduction in the levels of LDH and CK-MB in cardiomyocytes when compared with the H/R group (P<0.05 or 0.01). Additionally, it was notable that the reductions in LDH and CK-MB levels were more pronounced at higher LIQ doses, suggesting that LIQ pre-treatment effectively mitigated the damage to cardiomyocytes caused by H/R.

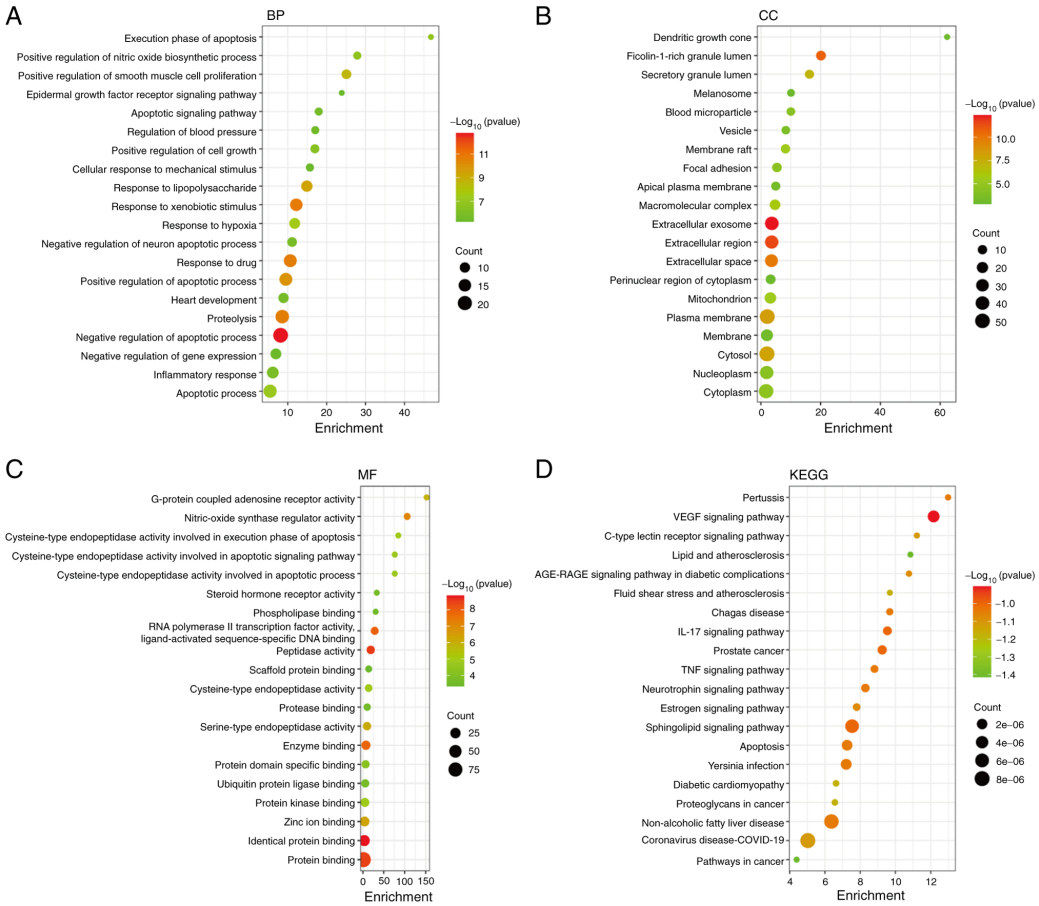

Figure 3. GO and KEGG analysis. (A-C) GO functional analysis and (D) KEGG pathway enrichment analysis of key LIQ anti-MIRI targets. GO, Gene Ontology; KEGG, Kyoto Encyclopedia of Genes and Genomes; LIQ, liquiritin; MIRI, myocardial ischemia-reperfusion injury; BP, biological process; CC, cellular component; MF, molecular function.

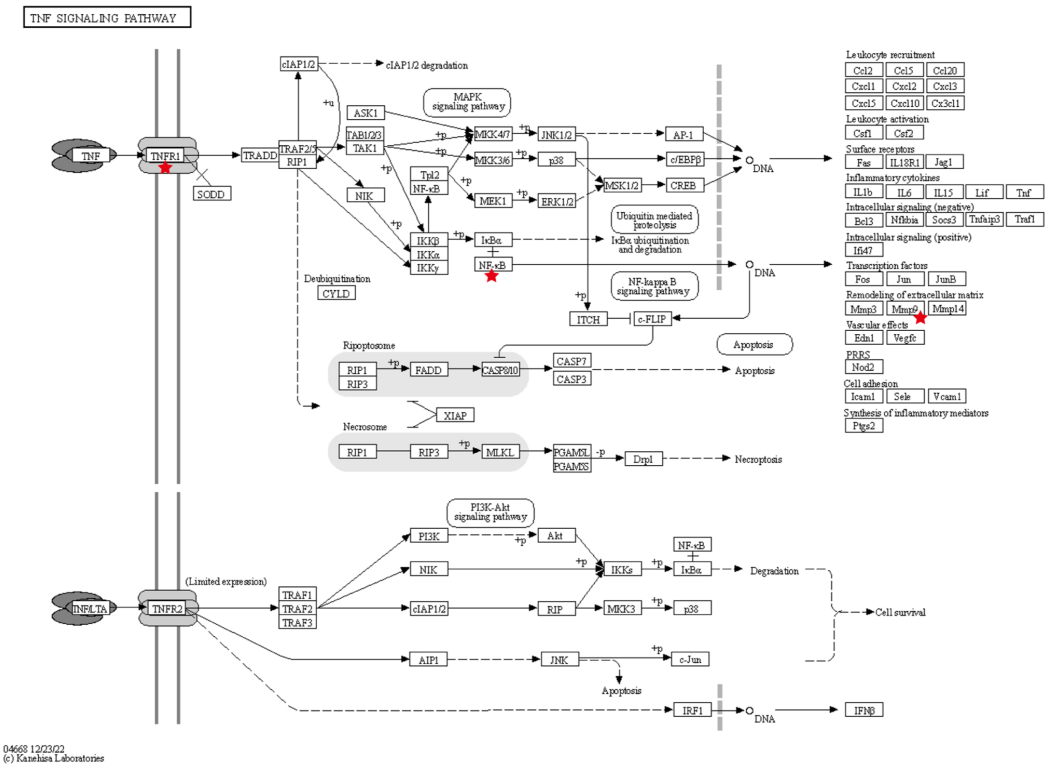

Figure 4. Demonstration of the TNF signaling pathway and the target to be tested. TNFR1, TNF-α receptor type 1; NF-κB, nuclear factor kappa-B; MMP9, Matrix metalloproteinase-9.

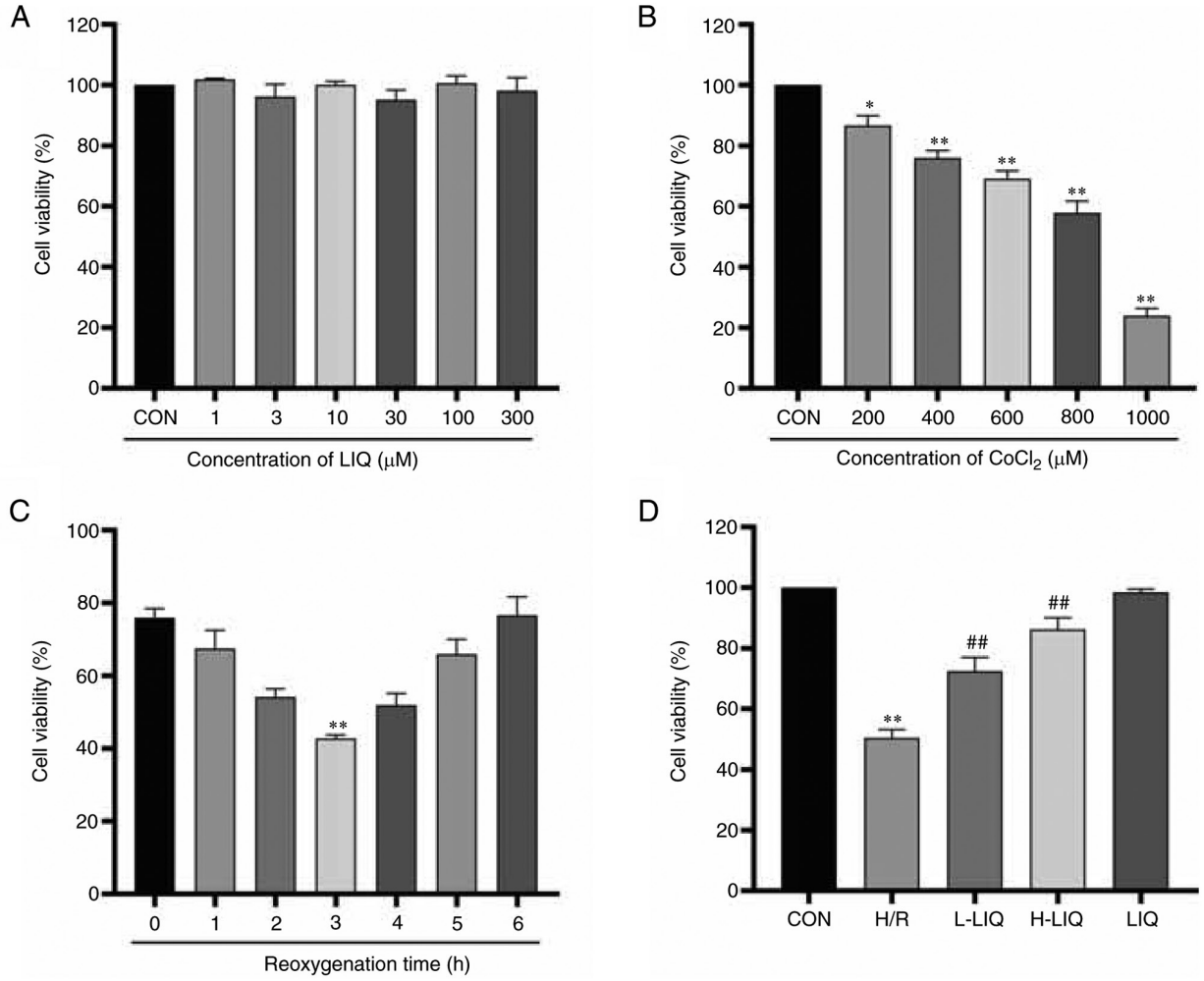

Figure 5. Effect of CoCl2 and LIQ on the viability of H9c2 cells by CCK-8 assay. H9c2 cells were incubated with different concentrations of (A) LIQ and (B) $CoCl_2$ for 24 h, followed by (C) reoxygenation. (D) The vitality of H9c2 cells in each group is shown by the CCK8 assay. Data are represented as mean ± standard error of mean. *P<0.05, **P<0.01 vs. CON; $^{\#\#}$P<0.01 vs. H/R group, n=3. LIQ, liquiritin; CON, control; H/R, hypoxia/reoxygenation; L-LIQ, 3 μmol/l; H-LIQ, 10 μmol/l.

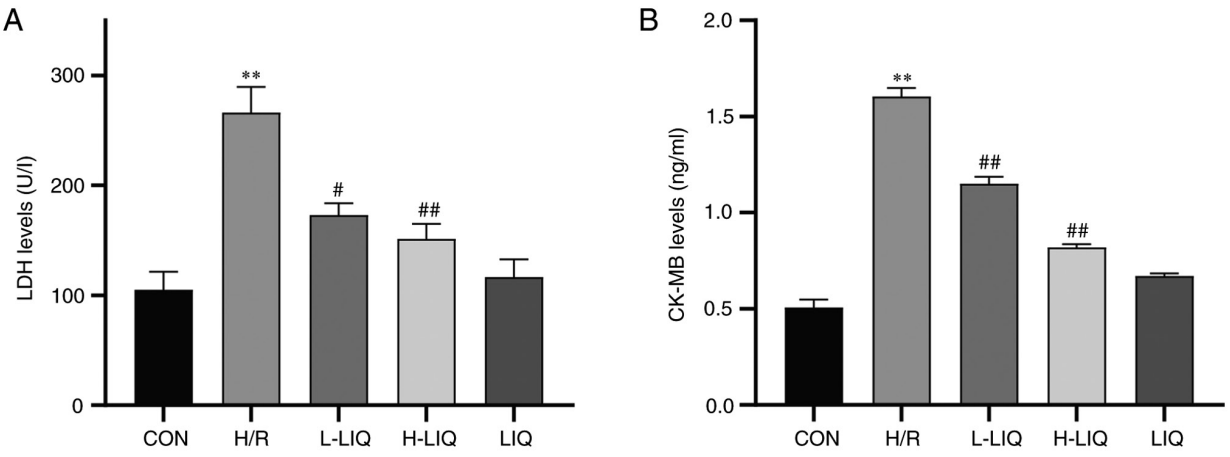

Figure 6. Effects of LIQ treatment on (A) LDH and (B) CK-MB levels in H/R-induced H9c2 cells. Data are represented as mean ± standard error of mean. **P<0.01 vs. CON; $^{\#}$P<0.05, $^{\#\#}$P<0.01 vs. H/R group, n=3. LIQ, liquiritin; LDH, lactated dehydrogenase; CK-MB, creatine kinase isoenzyme-MB; CON, control; H/R, hypoxia/reoxygenation; L-LIQ, 3 μmol/l; H-LIQ, 10 μmol/l.

Effect of LIQ on the levels of SOD, CAT, GSH-Px and MDA. As illustrated in Fig. 7, the levels of MDA, SOD, CAT and GSH-Px and can serve as indicators of oxidative stress damage. In comparison to the CON group, the H/R group displayed notably lower levels of SOD, CAT and GSH-Px (P<0.01), while the levels of MDA were significantly higher

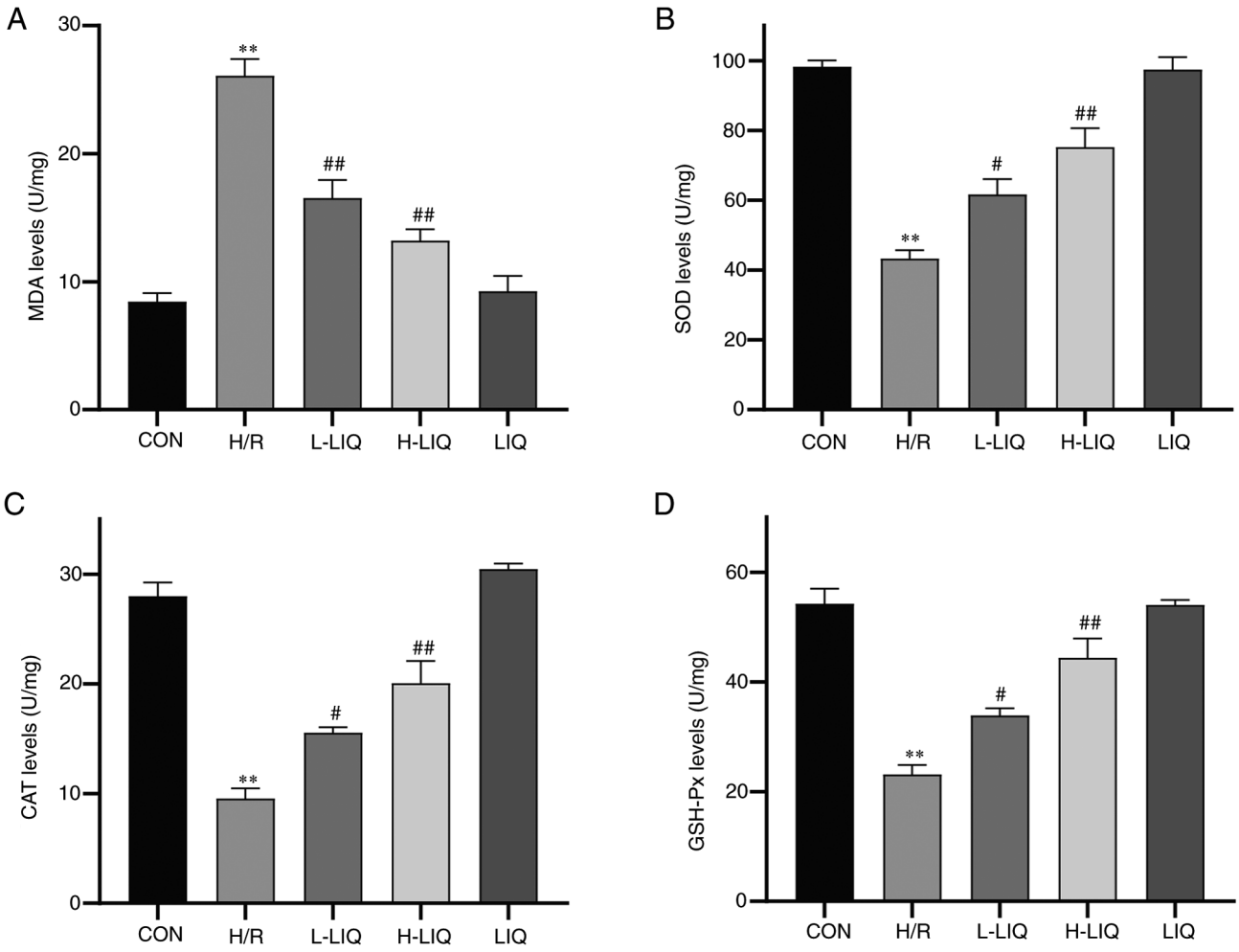

Figure 7. Effects of LIQ on H/R-induced levels of oxidative stress. (A) MDA, (B) SOD. (C) CAT and (D) GSH-Px levels. Data are represented as mean ± standard error of mean. **P<0.01 vs. CON; $^{\#}$P<0.05, $^{\#\#}$P<0.01 vs. H/R group, n=3. LIQ, liquiritin; H/R, hypoxia/reoxygenation; MDA, malondialdehyde; SOD, superoxide dismutase; CAT, catalase; GSH-Px, glutathione peroxidase; CON, control; H/R, hypoxia/reoxygenation; L-LIQ, 3 μmol/l; H-LIQ, 10 μmol/l.

(P<0.01). However, the pre-protective effect of LIQ alleviated the damage induced by H/R, as evidenced by significantly higher levels of SOD, CAT and GSH-Px in the LIQ group in comparison to the H/R group (P<0.05 or 0.01), along with significantly lower levels of MDA (P<0.01).

Effect of LIQ on ROS generation. The intracellular ROS level and the intensity of green fluorescence demonstrated a direct proportional relationship. As depicted in Fig. 8, the intracellular fluorescence intensity and ROS level in H9c2 cells within the H/R group were markedly higher than in the CON group (P<0.01). By contrast, the fluorescence intensity and ROS level in the LIQ group were significantly lower than those in the H/R group (P<0.01). Additionally, it was observed that the antagonistic effect on H/R injury became more pronounced with higher doses of LIQ.

Effects of LIQ on MtMP. The extent of MtMP damage showed an inverse correlation with the aggregation of Rh123. As depicted in Fig. 9, the aggregation of Rh123 in H9c2 cells of the H/R group was significantly lower compared with the CON group, indicating substantial MtMP damage (P<0.01). In contrast, the aggregation of Rh123 in H9c2 cells was significantly increased in the LIQ-treated group compared with the H/R group (P<0.05 or 0.01). This suggests that LIQ can effectively reduce MtMP damage in H/R injury with a concentration-dependent effect. The higher the concentration, the more pronounced the effect.

Effects of LIQ on apoptosis. During the process of apoptosis, morphological abnormalities often manifest, including cell shrinkage, chromatin condensation, cell membrane rupture and nuclear fragmentation (18). To verify the presence of apoptosis, the morphology of abnormal cells was examined using Hoechst 33258 staining and fluorescence microscopy. In normal cells, the nuclei displayed uniform blue fluorescence, while apoptotic cells exhibited densely stained blue nuclei or fragmented densely stained blue nuclei.

As illustrated in Fig. 10, when compared with the CON group, cells in the H/R group exhibited pronounced apoptotic morphology when observed under fluorescence microscopy following ultraviolet light excitation (P<0.01). However, in the LIQ-treated group, the apoptotic morphology was significantly reduced compared with the H/R group (P<0.01), indicating that LIQ attenuated H/R-induced apoptosis and enhanced the survival rate of H9c2 cells.

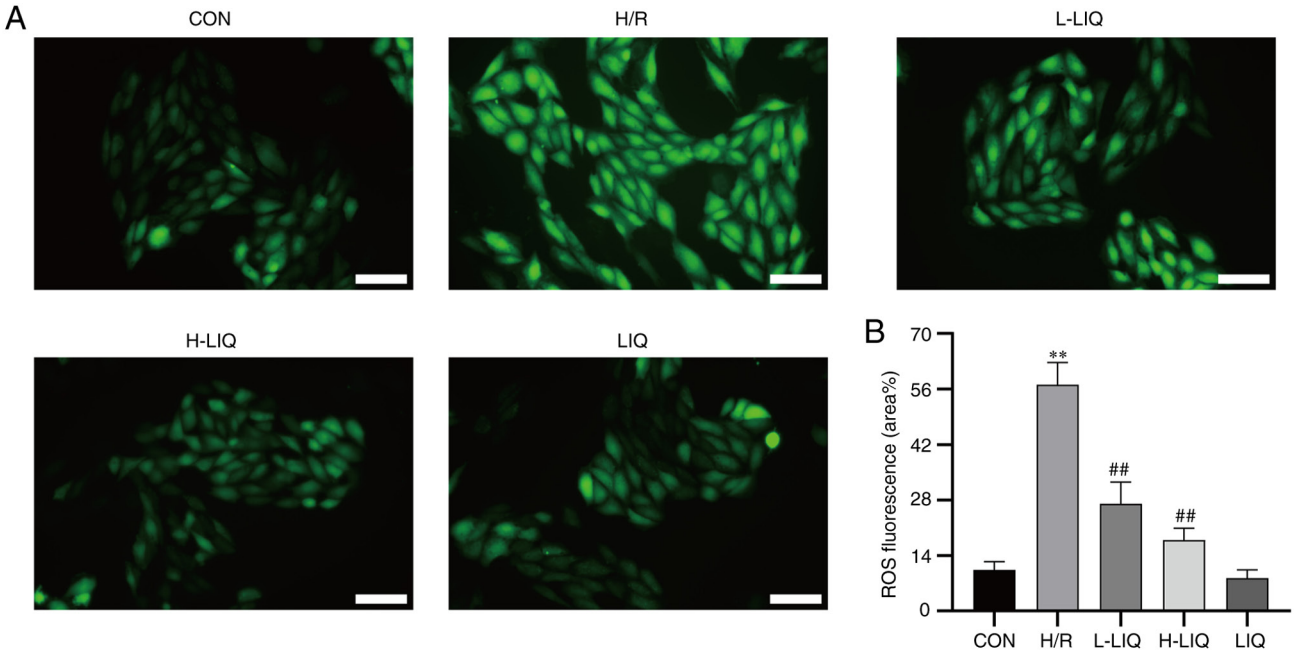

Figure 8. Effects of LIQ on H/R-induced levels of ROS. (A) Morphological changes of intracellular ROS (scale bar: 100 μm; magnification, x200). (B) Statistical analysis of ROS fluorescence. Data are represented as mean ± standard error of mean. **P<0.01 vs. CON; $^{\#\#}$P<0.01 vs. H/R group, n=3. LIQ, liquiritin; H/R, hypoxia/reoxygenation; ROS, reactive oxygen species; CON, control; H/R, hypoxia/reoxygenation; L-LIQ, 3 μmol/l; H-LIQ, 10 μmol/l.

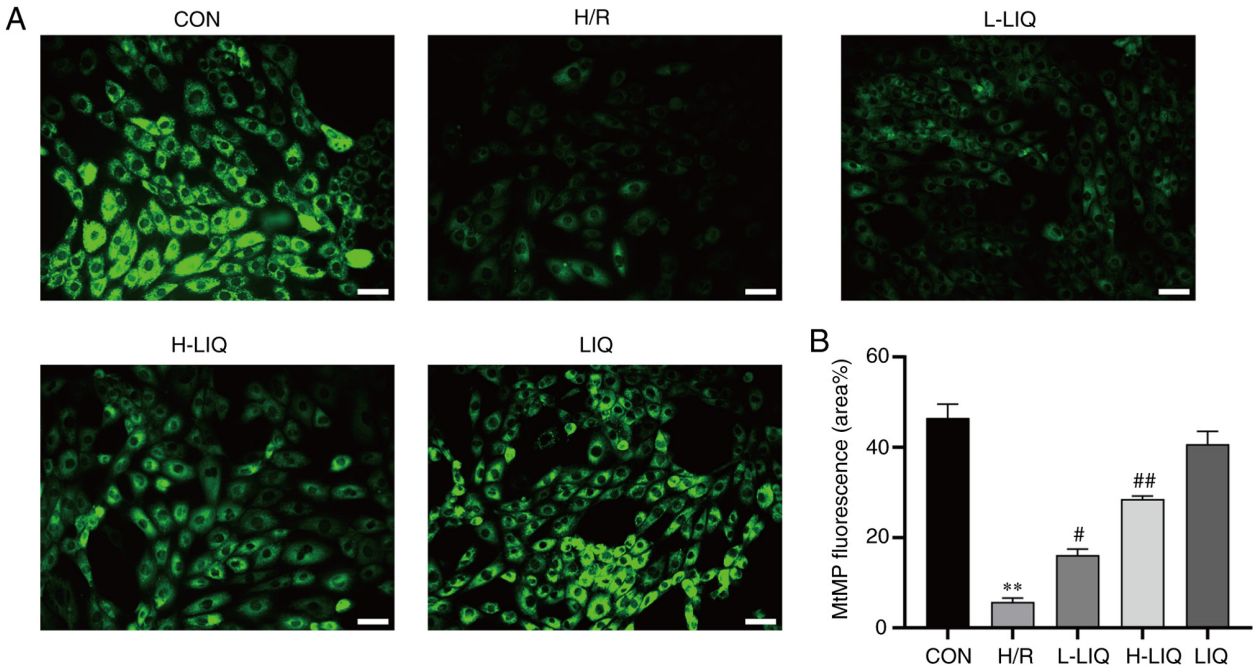

Figure 9. Effects of LIQ on H/R-induced mitochondrial damage in H9c2 cells. (A) Morphological changes of mitochondria were observed by Rhodamine 123 (scale bar, 100 μm; magnification, x200). (B) Statistical analysis of mitochondrial fluorescence was presented. Data are represented as mean ± standard error of mean. **P<0.01 vs. CON; $^{\#}$P<0.05, $^{\#\#}$P<0.01 vs. H/R group, n=3. LIQ, liquiritin; H/R, hypoxia/reoxygenation; CON, control; H/R, hypoxia/reoxygenation; L-LIQ, 3 μmol/l; H-LIQ, 10 μmol/l; MtMP, mitochondrial membrane potential.

Effects of LIQ on the levels of TNF-α and IL-6. The results depicted in Fig. 11 indicated a significant increase in the secretion levels of TNF-α and IL-6 in the H/R group when compared with the CON group (P<0.01). However, LIQ treatment notably reduced the secretion levels of TNF-α and IL-6 (P<0.05 or 0.01). These findings suggested that LIQ can effectively mitigate the inflammatory damage induced by H/R, with a more pronounced antagonistic effect observed at higher doses.

Effect of LIQ on the protein expression levels of TNFR1, p-NF-κB/NF-κB and MMP9. The results of western blotting, showing TNFR1, p-NF-κB/NF-κB and MMP9 protein expression in H9c2 cells, are presented in Fig. 12. The expression

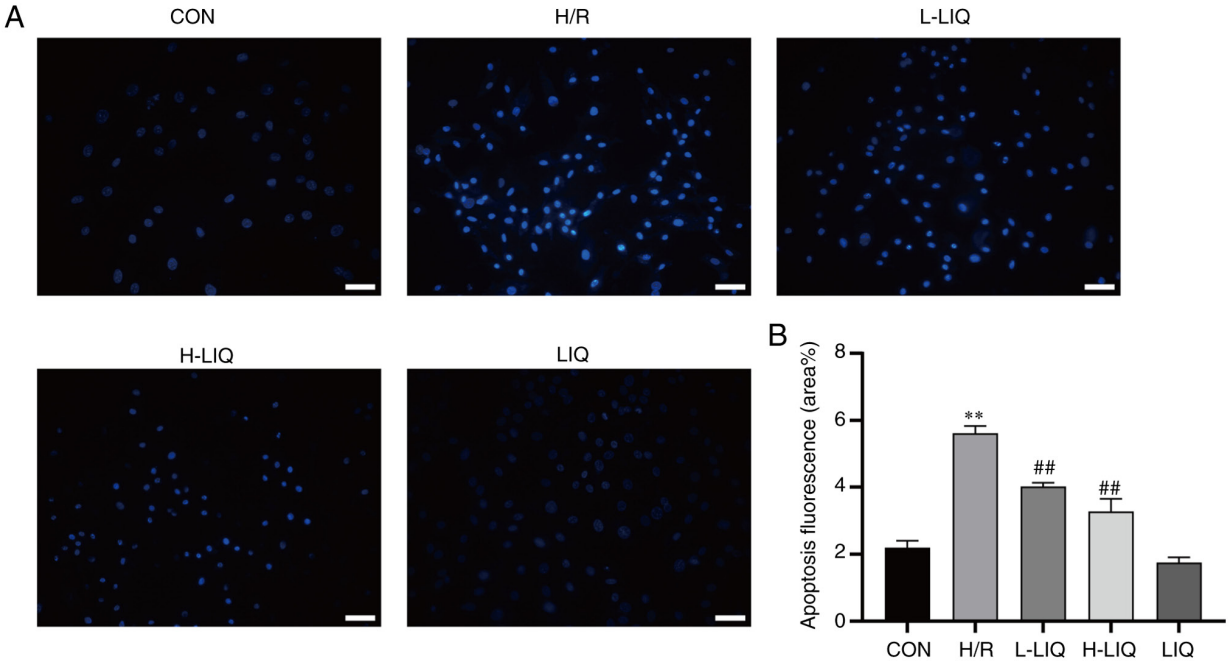

Figure 10. Effects of LIQ on H/R-induced apoptosis in H9c2 cells. (A) Cardiomyocyte apoptosis was assessed by Hoechst 33258 staining (scale bar, 100 μm; magnification, x200). (B) Statistical analysis of apoptosis fluorescence was presented. Data are represented as mean ± standard error of mean. **P<0.01 vs. CON; $^{\#\#}$P<0.01 vs. H/R group, n=3. LIQ, liquiritin; H/R, hypoxia/reoxygenation; CON, control; H/R, hypoxia/reoxygenation; L-LIQ, 3 μmol/l; H-LIQ, 10 μmol/l;

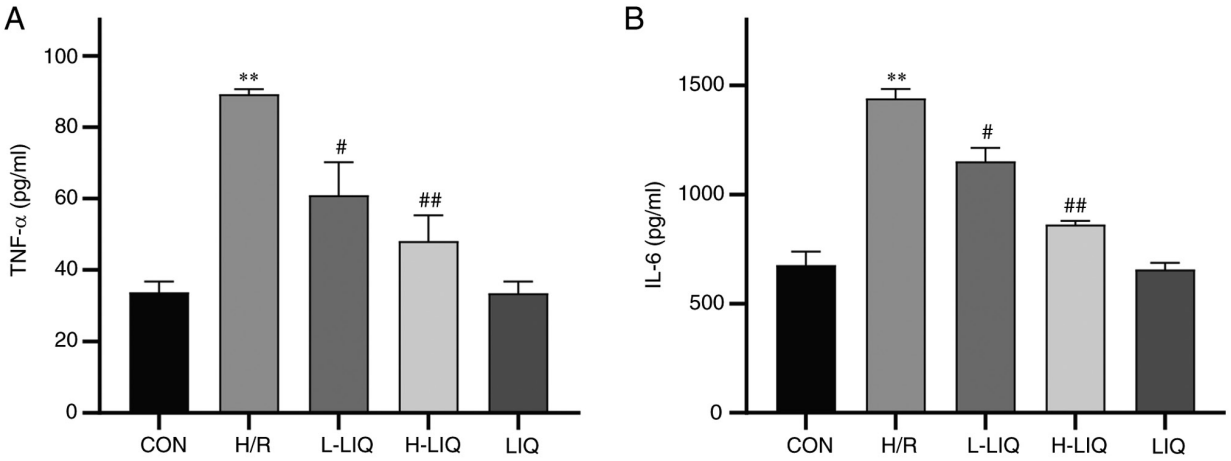

Figure 11. Effect of LIQ treatment on H/R-induced TNF-α (A) and IL-6 (B) levels in H9c2 cells injury. Data are represented as mean ± standard error of mean. **P<0.01 vs. CON; $^{\#}$P<0.05, $^{\#\#}$P<0.01 vs. H/R group, n=3. LIQ, liquiritin; H/R, hypoxia/reoxygenation; CON, control; H/R, hypoxia/reoxygenation; L-LIQ, 3 μmol/l; H-LIQ, 10 μmol/l.

levels of TNFR1, p-NF-κB/NF-κB and MMP9 proteins were markedly higher in the H/R group compared with the CON group (P<0.01). However, in the LIQ-treated group, the expression levels of these proteins were significantly lower than in the H/R group, demonstrating significant differences (P<0.05 or 0.01). These findings indicated that LIQ effectively mitigated the abnormally elevated expression of TNFR1, p-NF-κB/NF-κB and MMP9 proteins.

Discussion

The present study proposes the use of network pharmacology to predict potential targets and mechanisms of LIQ in the treatment of MIRI. An *in vitro* H/R model was employed to simulate MIRI and cellular experiments were conducted to validate the protective mechanisms of LIQ on H/R-injured cardiomyocytes. The investigation focused on various perspectives, including oxidative stress, inflammation, apoptosis, mitochondria and molecular mechanisms (Fig. 13). These observations suggested that LIQ exhibited multiple biological properties, implying its potential as an effective therapeutic approach or adjunct in the treatment of MIRI.

The physicochemical parameters of LIQ, which are crucial for subsequent drug analysis, were sourced from the TCMSP database. These parameters highlighted the potential of LIQ as a candidate for effective drug development. The Venn diagram

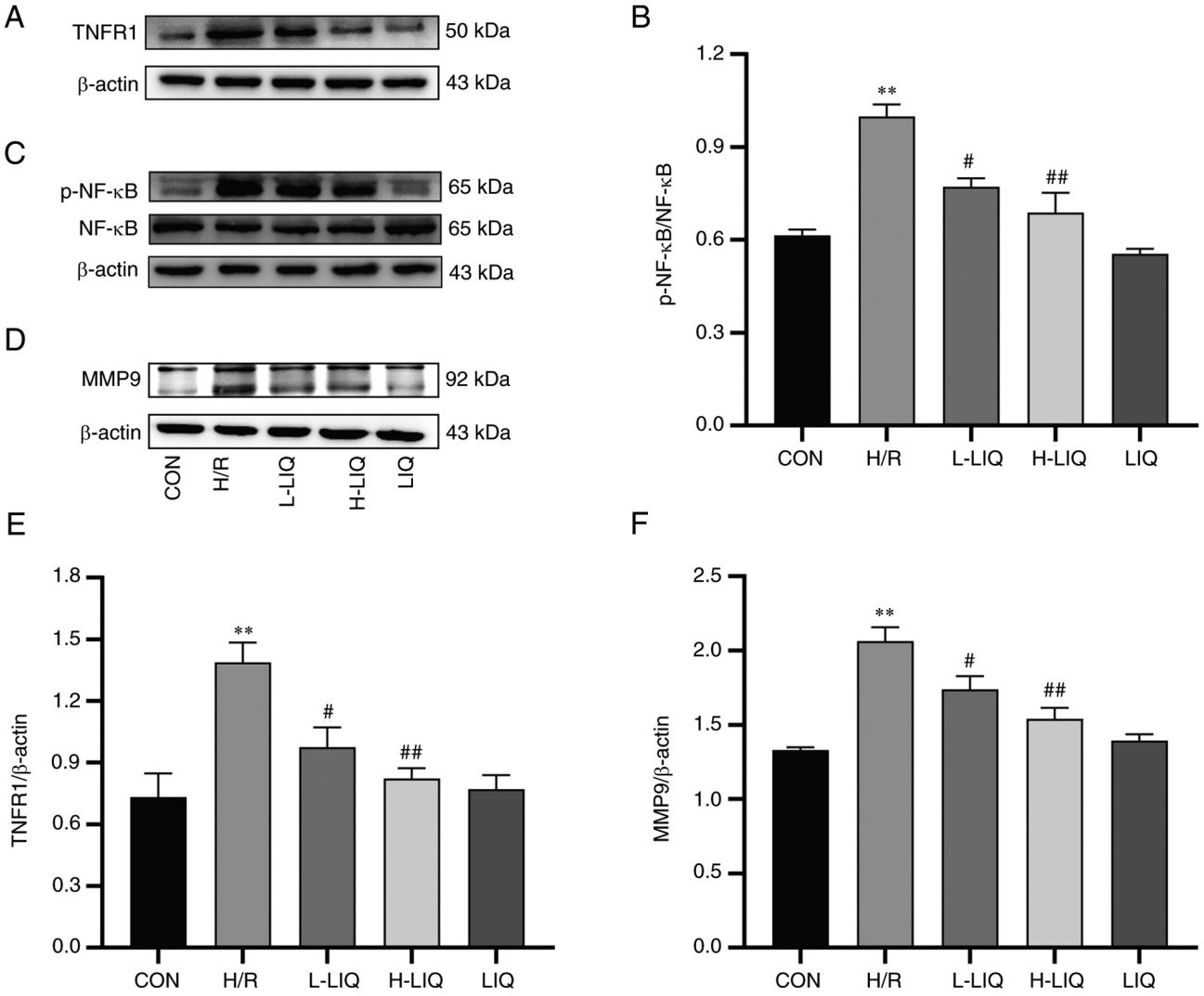

Figure 12. Effects of LIQ on the (A and E) TNFR1, (C and B) p-NF-κB/NF-κB and (D and F) MMP9 protein expressions. Data are represented as mean ± standard error of mean. **P<0.01 vs. CON; $^{\#}$P<0.05, $^{\#\#}$P<0.01 vs. H/R group, n=3. LIQ, liquiritin; TNFR1, TNF-α receptor type 1; p-, phosphorylated; CON, control; H/R, hypoxia/reoxygenation; L-LIQ, 3 μmol/l; H-LIQ, 10 μmol/l.

revealed that LIQ may target inflammation through 99 identified targets. By mining core targets, the present study was able to pinpoint more critical targets among the common ones, including AKT1, CASP3, ALB, SRC and MMP9, from the 95 targets identified through Cytoscape analysis. Additionally, GO and KEGG analyses suggested that the anti-MIRI effects of LIQ were associated with multiple mechanisms, such as oxidative stress, apoptosis, mitochondria and inflammation. These network pharmacology findings underscore the integrative nature of Chinese medicine.

H9c2, a rodent ventricular cardiomyocyte cell line with biochemical and physiological properties similar to human cardiomyocytes, has become a preferred choice for *in vitro* studies investigating the electrophysiological and biochemical characteristics of myocardial tissues (19). The most commonly utilized method for inducing hypoxia in laboratory settings is chemical hypoxia-induced by $CoCl_2$. This method offers advantages in terms of cost-effectiveness and convenience compared with physical hypoxia methods. The mechanism involves the replacement of Fe^{2+} in prolyl hydroxylase (PHD) with Co^{2+} from $CoCl_2$, resulting in the inactivation of PHD. Consequently, the degradation of hypoxia-inducible factor (HIF) is blocked. HIF plays a critical role in regulating oxygen homeostasis in mammals. Notably, even under normoxic conditions, HIF degradation is halted, remaining stable for several hours. This experimental stability provides operators with more time for sample manipulation and analysis (20). The present study employed the CCK-8 assay to assess cell viability and determine the optimal hypoxic concentration and reoxygenation time. Based on the results, it established the H/R model by subjecting cells to 400 μmol/l $CoCl_2$-induced hypoxia, followed by reoxygenation for 3 h.

The levels of LDH and CK-MB released served as indicators of cell damage and the integrity of the cell membrane. These enzymes are released when the cell membrane is disrupted and therefore their levels reflect the extent of damage and cellular necrosis (21). The results further substantiate this observation, as they revealed a significant increase in LDH and CK-MB release following H/R injury when compared with the CON group. However, pre-treatment with LIQ mitigated this injury.

Oxidative stress is a pivotal pathological mechanism within the complex network of systems involved in H/R pathology (22). The normal balance between intracellular ROS

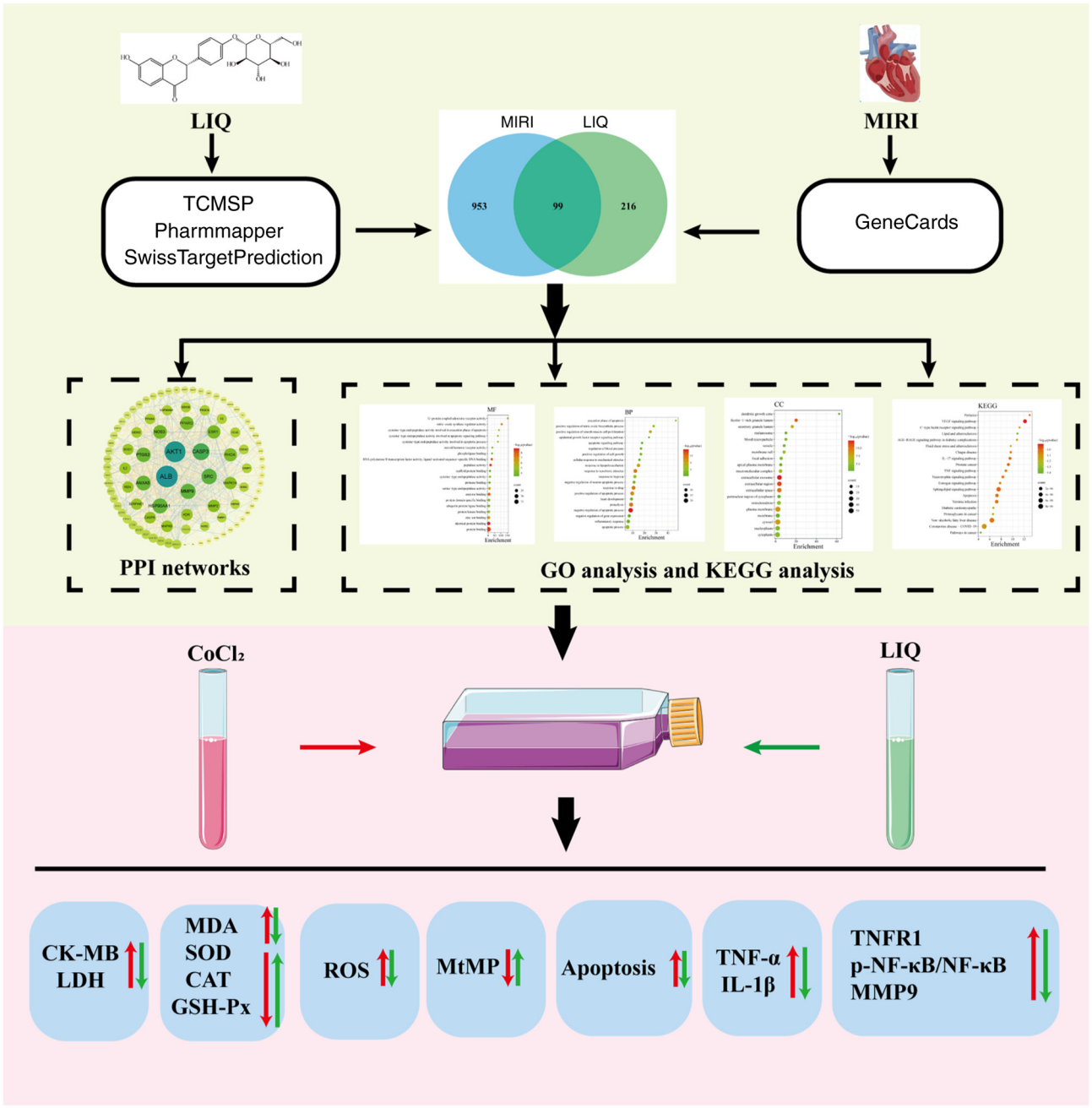

Figure 13. Workflow diagram for studying the mechanism of LIQ resistance to H/R-induced damage. LIQ, liquiritin; H/R, hypoxia/reoxygenation; L-LIQ, 3 μmol/l; H-LIQ, 10 μmol/l. MIRI, myocardial ischemia-reperfusion injury; TCMSP, Traditional Chinese Medicine Systems Pharmacology Database; PPI, protein-protein interaction; GO, Gene Ontology; KEGG, Kyoto Encyclopedia of Genes and Genomes; CK-MB, creatine kinase isoenzyme-MB; LDH, lactated dehydrogenase; MDA, malondialdehyde; SOD, superoxide dismutase; CAT, catalase; GSH-Px, glutathione peroxidase; ROS, reactive oxygen species; TNFR1, TNF-α receptor type 1; p-, phosphorylated; MtMP, mitochondrial membrane potential.

production and the activity of oxidant-scavenging enzyme systems (such as CAT, SOD and GSH) is disrupted, leading to oxidative stress (23). Hypoxia induces a reduction in endogenous ROS scavengers and an increase in ROS production due to residual oxygen, resulting in ROS accumulation in the myocardium. Upon reperfusion, the sudden influx of excessive oxygen further exacerbates ROS levels, causing oxidative damage to cellular structures, including lipid peroxidation (24). Among the sources of ROS in cardiac myocytes, mitochondria are the primary contributors. Insufficient oxygen supply disrupts mitochondrial coupling, leading to abnormal electron transfer in the mitochondrial aerobic metabolic respiratory chain. The subsequent elevation in ROS levels damages cells and can trigger apoptosis (25). MDA, the most crucial product of lipid peroxidation, reflects the extent of lipid peroxidation and the severity of cellular exposure to free radicals, making it a commonly used indicator of oxidative stress. SOD, CAT and GSH-Px, integral components of the oxidant scavenger enzyme system, constitute the primary cellular defense against oxidative damage and their activity reflects the ability of the body to eliminate excess ROS (24). The findings of the present study align with the aforementioned processes. As depicted in Figs. 7 and 8, H/R-treated H9c2 cells exhibited a significant increase in MDA and ROS levels, along with decreased SOD,

CAT and GSH-Px activity. Conversely, pre-treatment with LIQ yielded the opposite results.

Cardiomyocytes house numerous mitochondria, comprising ~30% of their volume. These mitochondria play a pivotal role in providing adenosine triphosphate to the cell through glucose degradation and other pathways (26), rendering them essential for maintaining cardiomyocyte function (27). Mitochondria are intricately involved in the complex pathological mechanisms of H/R injury. Significant factors include excessive ROS production, dysfunction in the electron transport chain, dysregulation of calcium homeostasis, abnormal opening of the mitochondrial permeability transition pore (mPTP), depolarization of MtMP and inappropriate activation of apoptosis (28). During myocardial hypoxia, there is a gradual impairment of mitochondrial electron transport system function and compromised mitochondrial energy metabolism (29). Although energy metabolism can be restored during reperfusion, early ROS accumulation can promote the opening of the mPTP, leading to MtMP collapse and ultimately triggering apoptosis (30). This underscores the critical role of mitochondrial damage in the progression of MIRI to heart failure (26). The present study used Rhodamine 123, a cationic fluorescent dye designed specifically to monitor mitochondrial function in living cells (31). The findings indicated that LIQ pre-treatment improved mitochondrial function, thus protecting H9c2 cells from H/R-induced damage.

Apoptosis is recognized as a significant characteristic in the pathogenesis of MIRI (32) and a primary mode of cell death (33) within the complex pathophysiological processes involved. A previous study has indicated that myocardial cells undergo apoptosis during hypoxia and reperfusion exacerbates its severity (34). The current study demonstrated that LIQ effectively reduced apoptosis levels, thus emphasizing its anti-apoptotic effect. During H/R injury, a reciprocal causal relationship exists between inflammation and apoptosis (35).

Numerous studies have highlighted the crucial regulatory role of the inflammatory response in H/R injury. Hypoxic necrotic cardiomyocytes trigger the transcriptional activity of inflammatory factors, including TNF-α and IL-6, which further exacerbates the inflammatory response (36,37). The findings of the present study align with prior research, demonstrating that H/R injury induced the release of TNF-α and IL-6 in cardiomyocytes, while LIQ pre-treatment significantly inhibited the abnormal expression of TNF-α and IL-6. Moreover, the increase in TNF-α activated xanthine oxidase, leading to ROS production and upregulation of inflammatory factor expression, thereby intensifying the inflammatory response. These processes not only worsen myocardial MIRI but also contributed to structural remodeling of the ventricles, ultimately resulting in the deterioration of cardiac function (38).

The pharmacology section of the network analysis produced a PPI network, revealing 95 common targets for LIQ and MIRI. Among these targets, AKT1, CASP3, ALB, SRC and MMP9 were identified as core predicted targets. KEGG analysis indicated a close association between LIQ and the TNF signaling pathway, with MMP9 identified as a core target within this pathway. Previous research has highlighted TNF as an effective pro-inflammatory cytokine that promotes and exacerbates inflammation through the induction of apoptosis or necroptosis (39,40). TNFR1 binds to TNF, activating the conventional NF-κB pathway (39). NF-κB regulation in cardiovascular diseases involves various pathological mechanisms, including immunity and inflammation (41).

Furthermore, MMP9, a member of the matrix metalloproteinase family, is implicated in the pathogenesis of various cardiovascular conditions. Research has shown elevated myocardial levels of MMP9 in both ischemic and non-ischemic cardiomyopathy (42-44). Alterations in NF-κB expression can also affect the regulation of the MMP9 gene (45). As a result, cellular experiments aimed at validating molecular mechanisms primarily revolve around the TNFR1/NF-κB/MMP9 signaling pathway.

TNFR1 is expressed in nearly all cell types, including cardiomyocytes and plays a crucial role in both pro-inflammatory and programmed cell death pathways (46). Therefore, TNFR1 was chosen as the focal point of the present study. In line with this, the results revealed an elevated expression of TNFR1 protein in $CoCl_2$-induced H/R injury in H9c2 cells.

Within the TNFR1 signaling pathway, the activation of NF-κB is a pivotal event that induces the expression of inflammatory genes and initiates an anti-apoptotic transcriptional program to counteract the pro-apoptotic pathway (47). Under normal conditions, the intracellular region of TNFR1 is inhibited by binding to the silencer of the death domain (SODD). When TNFR1 binds to TNF-α, SODD dissociates from TNFR1, enabling proteins such as TNF Receptor-Associated Death Domain, Receptor Interacting Protein 1, TNF Receptor-Associated Factor 2 and other proteins to assemble and form complex I. In its inactive state, the p50/65 dimer of NF-κB is localized in the cytoplasm and concealed by IκB, which binds to the p50/65 dimer, forming a trimer. Activation of complex I leads to the activation of the IκB kinase complex (Ikk), which phosphorylates the serine residue at the N-terminal end of IκB. Subsequently, the phosphorylated IκB protein undergoes ubiquitination and degradation, thereby releasing the active p50/65 dimer. Consequently, NF-κB is liberated and translocates from the cytoplasm to the nucleus (48-50), where it acts as a transcription factor, binding to specific DNA sequences and inducing the transcription and expression of relevant genes (51,52). A Previous study has identified a regulatory, structural domain of NF-κB in the 670 bp promoter region of MMP-9 (53). TNF-α induces MMP9 expression in mammalian cells through the NF-κB signaling pathway and activates the MMP9 promoter at varying TNF-α concentrations (54). MMP9 has been implicated in myocardial injury following AMI. During cardiac remodeling following AMI, MMP9 participates in extracellular matrix degradation, increases capillary permeability and activates inflammatory mediators. Moreover, in animal models of cardiovascular diseases, elevated myocardial MMP9 expression has been observed and the deletion or inhibition of MMP9 has shown beneficial effects (55). The present study also demonstrated that H/R significantly increased NF-κB phosphorylation and MMP9 expression and LIQ pre-treatment effectively alleviated their upregulation.

While the present study showed the beneficial effects of LIQ in mitigating H/R injury, it is important to acknowledge certain limitations. First, although H9c2 cells share morphological features and signaling pathway components with primary cardiomyocytes (56,57), they do not fully

replicate the complex regulatory processes that occur in the heart *in vivo*. Hence, further validation through *in vivo* experiments is warranted. Additionally, the number of targets validated in the present study was limited. Further investigation is necessary to confirm the regulatory effects of LIQ on other crucial targets involved in H/R injury. Another limitation of the present study is the absence of established positive controls, which were not included due to the previously established cardiac protective effect of LIQ using such controls (15). This aspect will be further investigated in our future research.

The present study employed a combination of network pharmacology and cellular experiments to illustrate that LIQ has the potential to mitigate MIRI and provide protection to the heart. It accomplished this by activating the TNFR1/NF-κB/MMP9 signaling pathway, inhibiting oxidative stress, enhancing MtMP regulation, managing inflammation and suppressing apoptosis. These findings enhance our comprehension of the pharmacological mechanism of LIQ and introduce a novel therapeutic approach for the clinical treatment of AMI.

Acknowledgements

Not applicable.

Funding

The present study was supported by the Research Foundation of Natural Science Foundation of Hebei Province Youth Project (grant no. H2021423027), Hebei Province high-level talent funding project (grant no. C20231060) and The Hebei Natural Science Foundation (grant no. H2022423306).

Availability of data and materials

The datasets used and/or analyzed during the current study are available from the corresponding author on reasonable request.

Authors' contributions

HL, LB, SG, XH and HW were involved in the conception and planning of the current study. HL, LB, XS and XC performed the experiments. HL, XS and LB interpreted the data. HL, XC, YX and JS were involved in the data analysis. XC, YX, JS and YL provided guidance for software and figures. HL wrote the original draft. LB, XS, XC, MZ, YL, XH, SG and HW reviewed and edited the manuscript. XH, SG and HW supervised the project. SG identified resources. HL and SG confirm the authenticity of all the raw data. All authors have read and approved the final version of the manuscript.

Ethics approval and consent to participate

Not applicable.

Patient consent for publication

Not applicable.

Competing interests

The authors declare that they have no competing interests.

References

1. Pollard TJ: The acute myocardial infarction. Prim Care 27: 631-649, 2000.
2. Eltzschig HK, Bonney SK and Eckle T: Attenuating myocardial ischemia by targeting A2B adenosine receptors. Trends Mol Med 19: 345-354, 2013.
3. Yang H, Wang C, Zhang L, Lv J and Ni H: Rutin alleviates hypoxia/reoxygenation-induced injury in myocardial cells by up-regulating SIRT1 expression. Chem Biol Interact 297: 44-49, 2019.
4. Zhang T, Zhang Y, Cui M, Jin L, Wang Y, Lv F, Liu Y, Zheng W, Shang H, Zhang J, *et al*: CaMKII is a RIP3 substrate mediating ischemia- and oxidative stress-induced myocardial necroptosis. Nat Med 22: 175-182, 2016.
5. Murphy E and Steenbergen C: Mechanisms underlying acute protection from cardiac ischemia-reperfusion injury. Physiol Rev 88: 581-609, 2008.
6. Du L, Shen T, Liu B, Zhang Y, Zhao C, Jia N, Wang Q and He Q: Shock Wave Therapy Promotes Cardiomyocyte Autophagy and Survival during Hypoxia. Cell Physiol Biochem 42: 673-684, 2017.
7. Gao X, Zhang H, Zhuang W, Yuan G, Sun T, Jiang X, Zhou Z, Yuan H, Zhang Z and Dong H: PEDF and PEDF-derived peptide 44mer protect cardiomyocytes against hypoxia-induced apoptosis and necroptosis via anti-oxidative effect. Sci Rep 4: 5637, 2014.
8. Yao H, Xie Q, He Q, Zeng L, Long J, Gong Y, Li X, Li X, Liu W, Xu Z, *et al*: Pretreatment with panaxatriol saponin attenuates mitochondrial apoptosis and oxidative stress to facilitate treatment of myocardial ischemia-reperfusion injury via the regulation of Keap1/Nrf2 activity. Oxid Med Cell Longev 2022: 9626703, 2022.
9. Pastorino G, Cornara L, Soares S, Rodrigues F and Oliveira M: Liquorice (Glycyrrhiza glabra): A phytochemical and pharmacological review. Phytother Res 32: 2323-2339, 2018.
10. Fan S, Gu K, Wu Y, Luo H, Wang Y, Zhang T, Wang X, Zhang Y and Li Y: Liquiritinapioside-A mineralocorticoid-like substance from liquorice. Food Chem 289: 419-425, 2019.
11. Hou Y and Jiang JG: Origin and concept of medicine food homology and its application in modern functional foods. Food Funct 4: 1727-1741, 2013.
12. Zhang Y, Zhang L, Zhang Y, Xu JJ, Sun LL and Li SZ: The protective role of liquiritin in high fructose-induced myocardial fibrosis via inhibiting NF-κB and MAPK signaling pathway. Biomed Pharmacother 84: 1337-1349, 2016.
13. Mou SQ, Zhou ZY, Feng H, Zhang N, Lin Z, Aiyasiding X, Li WJ, Ding W, Liao HH, Bian ZY and Tang QZ: Liquiritin attenuates lipopolysaccharides-induced cardiomyocyte injury via an AMP-Activated protein kinase-dependent signaling pathway. Front Pharmacol 12: 648688, 2021.
14. Thu VT, Yen NTH and Ly NTH: Liquiritin from radix glycyrrhizae protects cardiac mitochondria from Hypoxia/Reoxygenation damage. J Anal Methods Chem 2021: 1857464, 2021.
15. Han X, Yang Y, Zhang M, Li L, Xue Y, Jia Q, Wang X and Guan S: Liquiritin Protects against cardiac fibrosis after myocardial infarction by inhibiting CCL5 expression and the NF-kappaB signaling pathway. Drug Des Devel Ther 16: 4111-4125, 2022.
16. Boezio B, Audouze K, Ducrot P and Taboureau O: Network-based approaches in pharmacology. Mol Inform: 36, 2017 doi: 10.1002/minf.201700048.
17. Otasek D, Morris JH, Bouças J, Pico AR and Demchak B: Cytoscape Automation: Empowering workflow-based network analysis. Genome biology 20: 185, 2019.
18. Hu X, Jiao R, Li H, Wang X, Lyu H, Gao X, Xu F, Li Z, Hua H and Li D: Antiproliferative hydrogen sulfide releasing evodiamine derivatives and their apoptosis inducing properties. Eur J Med Chem 151: 376-388, 2018.
19. Fang Z, Luo W and Luo Y: Protective effect of α-mangostin against $CoCl_2$-induced apoptosis by suppressing oxidative stress in H9c2 rat cardiomyoblasts. Mol Med Rep 17: 6697-6704, 2018.
20. Munoz-Sanchez J and Chanez-Cardenas ME: The use of cobalt chloride as a chemical hypoxia model. J Appl Toxicol 39: 556-570, 2019.

21. Amani M, Jeddi S, Ahmadiasl N, Usefzade N and Zaman J: Effect of HEMADO on level of CK-MB and LDH enzymes after ischemia/reperfusion injury in isolated rat heart. Bioimpacts 3: 101-104, 2013.
22. Raedschelders K, Ansley DM and Chen DD: The cellular and molecular origin of reactive oxygen species generation during myocardial ischemia and reperfusion. Pharmacol Ther 133: 230-255, 2012.
23. Farias JG, Molina VM, Carrasco RA, Zepeda AB, Figueroa E, Letelier P and Castillo RL: Antioxidant therapeutic strategies for cardiovascular conditions associated with oxidative stress. Nutrients 9: 996, 2017.
24. Rodrigo R: Prevention of postoperative atrial fibrillation: Novel and safe strategy based on the modulation of the antioxidant system. Front Physiol 3: 93, 2012.
25. Xiang M, Lu Y, Xin L, Gao J, Shang C, Jiang Z, Lin H, Fang X, Qu Y, Wang Y, *et al*: Role of oxidative stress in reperfusion following myocardial ischemia and its treatments. Oxid Med Cell Longev 2021: 6614009, 2021.
26. Marin W, Marin D, Ao X and Liu Y: Mitochondria as a therapeutic target for cardiac ischemia-reperfusion injury (Review). Int J Mol Med 47: 485-499, 2021.
27. Carreira RS, Lee P and Gottlieb RA: Mitochondrial therapeutics for cardioprotection. Curr Pharm Des 17: 2017-2035, 2011.
28. Su X, Zhou M, Li Y, An N, Yang F, Zhang G, Xu L, Chen H, Wu H and Xing Y: Mitochondrial damage in myocardial Ischemia/Reperfusion injury and application of natural plant products. Oxid Med Cell Longev 2022: 8726564, 2022.
29. Lesnefsky EJ, Chen Q, Tandler B and Hoppel CL: Mitochondrial dysfunction and myocardial Ischemia-Reperfusion: Implications for novel therapies. Annu Rev Pharmacol Toxicol 57: 535-565, 2017.
30. Anzell AR, Maizy R, Przyklenk K and Sanderson TH: Mitochondrial quality control and disease: Insights into Ischemia-Reperfusion injury. Mol Neurobiol 55: 2547-2564, 2018.
31. Chazotte B: Labeling mitochondria with rhodamine 123. Cold Spring Harb Protoc 2011: 892-894, 2011.
32. Zhou H, Ma Q, Zhu P, Ren J, Reiter RJ and Chen Y: Protective role of melatonin in cardiac ischemia-reperfusion injury: From pathogenesis to targeted therapy. J Pineal Res: 64, 2018 doi: 10.1111/jpi.12471.
33. Yang J, Guo X, Yang J, Ding JW, Li S, Yang R, Fan ZX and Yang CJ: RP105 Protects against apoptosis in Ischemia/Reperfusion-Induced myocardial damage in rats by suppressing TLR4-Mediated signaling pathways. Cell Physiol Biochem 36: 2137-2148, 2015.
34. Li X, Hu X, Wang J, Xu W, Yi C, Ma R and Jiang H: Short-Term hesperidin pretreatment attenuates rat myocardial Ischemia/Reperfusion injury by inhibiting high mobility group box 1 protein expression via the PI3K/Akt Pathway. Cell Physiol Biochem 39: 1850-1862, 2016.
35. Zhang BF, Jiang H, Chen J, Guo X, Li Y, Hu Q and Yang S: Nobiletin ameliorates myocardial ischemia and reperfusion injury by attenuating endoplasmic reticulum stress-associated apoptosis through regulation of the PI3K/AKT signal pathway. Int Immunopharmacol 73: 98-107, 2019.
36. Yang Y, Lv J, Jiang S, Ma Z, Wang D, Hu W, Deng C, Fan C, Di S, Sun Y and Yi W: The emerging role of Toll-like receptor 4 in myocardial inflammation. Cell Death Dis 7: e2234, 2016.
37. Naidu BV, Farivar AS, Woolley SM, Grainger D, Verrier ED and Mulligan MS: Novel broad-spectrum chemokine inhibitor protects against lung ischemia-reperfusion injury. J Heart Lung Transplant 23: 128-134, 2004.
38. Chen L, Liu P, Feng X and Ma C: Salidroside suppressing LPS-induced myocardial injury by inhibiting ROS-mediated PI3K/Akt/mTOR pathway in vitro and in vivo. J Cell Mol Med 21: 3178-3189, 2017.
39. Ting AT and Bertrand MJM: More to Life than NF-κB in TNFR1 Signaling. Trends Immunol 37: 535-545, 2016.
40. Pasparakis M and Vandenabeele P: Necroptosis and its role in inflammation. Nature 517: 311-320, 2015.
41. Van der Heiden K, Cuhlmann S, Luong le A, Zakkar M and Evans PC: Role of nuclear factor kappaB in cardiovascular health and disease. Clin Sci (Lond) 118: 593-605, 2010.
42. Newby AC: Dual role of matrix metalloproteinases (matrixins) in intimal thickening and atherosclerotic plaque rupture. Physiol Rev 85: 1-31, 2005.
43. Spinale FG, Coker ML, Heung LJ, Bond BR, Gunasinghe HR, Etoh T, Goldberg AT, Zellner JL and Crumbley AJ: A matrix metalloproteinase induction/activation system exists in the human left ventricular myocardium and is upregulated in heart failure. Circulation 102: 1944-1949, 2000.
44. Spinale FG: Matrix metalloproteinase gene polymorphisms in heart failure: New pieces to the myocardial matrix puzzle. Eur Heart J 25: 631-633, 2004.
45. Luo X, Wu J and Wu G: PPARγ activation suppresses the expression of MMP9 by downregulating NF-κB post intracerebral hemorrhage. Neurosci Lett 752: 135770, 2021.
46. Kleinbongard P, Heusch G and Schulz R: TNFalpha in atherosclerosis, myocardial ischemia/reperfusion and heart failure. Pharmacol Ther 127: 295-314, 2010.
47. Hayden MS and Ghosh S: Regulation of NF-κB by TNF family cytokines. Semin Immunol 26: 253-266, 2014.
48. Hayden MS and Ghosh S: NF-κB, the first quarter-century: Remarkable progress and outstanding questions. Genes Dev 26: 203-234, 2012.
49. Blackwell K, Zhang L, Thomas GS, Sun S, Nakano H and Habelhah H: TRAF2 phosphorylation modulates tumor necrosis factor alpha-induced gene expression and cell resistance to apoptosis. Mol Cell Biol 29: 303-314, 2009.
50. Devin A, Cook A, Lin Y, Rodriguez Y, Kelliher M and Liu Z: The distinct roles of TRAF2 and RIP in IKK activation by TNF-R1: TRAF2 recruits IKK to TNF-R1 while RIP mediates IKK activation. Immunity 12: 419-429, 2000.
51. Wei Q, Tu Y, Zuo L, Zhao J, Chang Z, Zou Y and Qiu J: MiR-345-3p attenuates apoptosis and inflammation caused by oxidized low-density lipoprotein by targeting TRAF6 via TAK1/p38/NF-kB signaling in endothelial cells. Life Sci 241: 117142, 2020.
52. Howell JA and Bidwell GL III: Targeting the NF-κB pathway for therapy of ischemic stroke. Ther Deliv 11: 113-123, 2020.
53. Gum R, Lengyel E, Juarez J, Chen JH, Sato H, Seiki M and Boyd D: Stimulation of 92-kDa gelatinase B promoter activity by ras is mitogen-activated protein kinase kinase 1-independent and requires multiple transcription factor binding sites including closely spaced PEA3/ets and AP-1 sequences. J Biol Chem 271: 10672-10680, 1996.
54. Wu HT, Sie SS, Kuan TC and Lin CS: Identifying the regulative role of NF-κB binding sites within promoter region of human matrix metalloproteinase 9 (mmp-9) by TNF-α induction. Appl Biochem Biotechnol 169: 438-449, 2013.
55. Neri M, Riezzo I, Pascale N, Pomara C and Turillazzi E: Ischemia/Reperfusion Injury following Acute Myocardial Infarction: A critical issue for clinicians and forensic pathologists. Mediators Inflamm 2017: 7018393, 2017.
56. Hescheler J, Meyer R, Plant S, Krautwurst D, Rosenthal W and Schultz G: Morphological, biochemical, and electrophysiological characterization of a clonal cell (H9c2) line from rat heart. Circ Res 69: 1476-1486, 1991.
57. Zhu A, Wei X, Zhang Y, You T, Yao S, Yuan S, Xu H, Li F and Mao W: Propofol provides cardiac protection by suppressing the proteasome degradation of caveolin-3 in ischemic/reperfused rat hearts. J Cardiovasc Pharmacol 69: 170-177, 2017.